Highspeed Laser Micro Processing using Ultrashort Laser Pulses

Joerg SCHILLE [*1,2], Lutz SCHNEIDER[*1], Mathias MUELLER[*1], Udo LOESCHNER[*1], Nicholas GODDARD[*2], Patricia SCULLY[*2] and Horst EXNER[*1]

[*1] *University of Applied Sciences Mittweida, Technikumplatz 17, 09648 Mittweida, Germany.*
schille@hs-mittweida.de
[*2] *School of Chemical Engineering and Analytical Science, The University of Manchester, Oxford Road, Manchester, M13 9PL, United Kingdom.*

This paper discusses results obtained in highspeed laser micro processing of zirconium oxide ceramic and stainless steel. High-PRF (pulse repetition frequency) femtosecond laser systems were joined together with fast galvanometer scanner systems. A high average laser power (31.7 W) and fast scan speeds (17.1 m/s) were applied in order to increase material removal. The influence of average laser power, laser energy and repetition rate on both the volume ablation rate and the machining quality was studied. The maximum volume ablation rate for zirconium oxide was 70.3 µm³ per pulse, obtained with pulses of 5.9 µJ energy and 1.02 MHz. It is demonstrated that material removal on zirconium oxide will be strongly affected by heat. Stainless steel was irradiated with a maximum laser power of 31.7 W and various repetition rates. The maximum material removal rate was found to be 6.8 mm³ / min, achieved with laser pulses of 0.85 J/cm² fluence. The feasibility of the high-speed laser technology in micro processing is verified by machining examples. In addition, a demonstrator of 80 x 80 mm² was machined with a processing rate as high as 25 cm² / min.

DOI: 10.2961/jlmn.2014.02.0015
Keywords: ultrashort, micro processing, micromachining, highspeed, stainless steel, zirconium oxide, heat accumulation, particle shielding, high repetition rate, high-PRF

1. Introduction

The unique advantages of ultrashort laser pulses in micro processing are high efficiency, fast and localized energy deposition, and minimal thermal load on the work piece. These benefits suggest initially the great potential of the ultrashort pulse laser technology in micromachining with respect to accuracy, precision and machining quality. Moreover, by using the recently developed high average power high-PRF (pulse repetition frequency) femtosecond laser technology, a great leap can be made in terms of processing speed to overcome the technological drawback of limited throughput of the current ultrashort pulse lasers.

However, little research has been done up to now using high-PRF femtosecond laser systems in micro processing [1-7]. In these studies, heat accumulation and particle shielding have been identified as new interaction phenomena for ultrashort laser pulses, mainly caused by the short time interval between consecutive incident pulses. A further impact of these phenomena on material removal has to be expected by using higher laser power or higher repetition rates or both.

In this work, results obtained in highspeed laser micro processing of zirconium oxide and stainless steel plates are presented. High-PRF femtosecond laser systems with maximum laser power of 31.7 W were joined together with fast galvanometer scan systems. The laser beam was deflected across the sample surfaces by using raster scan methods. Maximum scan speeds as high as 17.1 m/s were applied in order to increase material removal. The impact of average laser power, laser energy and repetition rate on both the volume ablation rate and the machining quality is analyzed.

2. Fundamentals of high-PRF ultrashort pulse laser ablation

Recent studies investigating high-PRF femtosecond laser processing identified heat accumulation and particle shielding as major physical mechanisms in laser matter interaction [1, 6, 7].

With repetitive laser irradiation, there is a cyclic temperature variation at the sample surface. The surface temperature increases shortly after laser pulse absorption due to laser energy transfer from the electrons to the lattice, and cools down until the next laser pulse arrives. For high-PRF laser pulses with repetition rates higher than several hundreds of kilohertz, the time interval between individual pulses is less than the time required for the heat to diffuse out the focal volume. As a result, the residual thermal energy which does not diffuse away accumulates in the near-surface region, causing a surface temperature rise on the sample from pulse to pulse. Heat accumulation and temperature rise, however, highly depend on the time interval between consecutive incident laser pulses which is determined by the repetition rate.

The higher the repetition rate, the less the time for cooling down the sample surface and thus the next laser pulse interacts with a hotter surface. A higher surface temperature, in turn, will enhance the absorption of the next incident laser pulse [8], leading to a higher amount of deposited thermal energy. Moreover, the ablation threshold will be decrease with the higher repetition rates, causing increased ablation rates for pulses of the same energy but higher repetition rates [9]. This is potentially due to the fact that less energy will be needed to ablate the already heated material,

which is mainly induced by heat accumulation. From this it can be concluded that both laser beam absorption and subsequent material reaction are highly influenced by the substrate surface temperature.

Heat accumulation and surface temperature rise can be theoretically verified by a temperature simulation model introduced in [9]. In this model, thermal energy diffusion was determined by the heat diffusion length $\mathbf{l_d}$, which considerably depends on the time interval between two laser pulses and thus the repetition rate. For a specified number of laser pulses, this model calculates the surface temperature of a laser irradiated region at the end of a cooling cycle from pulse to pulse. Therefore, thermal energy diffusion of each individual laser pulse event is taken into account from pulse to pulse, which is in contrast to temperature calculations presented elsewhere [10, 11].

In this work, a limited number of incident laser pulses have been used for modeling in order to evaluate the thermal effect on material ablation induced by multiple femtosecond laser irradiations in the raster scan processing regime. For example, Fig. 1 illustrates schematically heat affected areas obtained on stainless steel for the time interval equal to five periods between the laser pulses. The repetition rate was varied between 51 kHz, 205 kHz and 1.02 MHz, leading to heat diffusion lengths of 17.5 µm, 8.7 µm, and 3.9 µm, respectively.

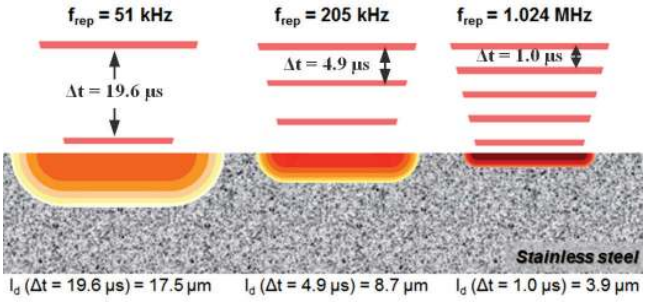

Fig. 1: Schematic of heat affected areas as obtained in stainless steel with 5 consecutive irradiated laser pulses of different repetition rates; the heat diffusion lengths $\mathbf{l_d}$ for the resulting time intervals between two pulses $\mathbf{\Delta t}$ are presented.

In Fig. 1 it can be seen that the thermal energy deposited by the previously irradiated pulses diffuses in larger areas when the fifth pulse irradiates. Moreover, it is observable for pulses at the higher repetition rate and thus the shorter time interval $\mathbf{\Delta t}$ that the thermal energy deposited by every individual pulse diffuses in a significantly smaller area, compared to pulses of the lower repetition rates. As a result, pulses of higher repetition rate will potentially irradiate a hotter surface, which is induced by accumulation of heat in the near- surface area.

The increase of the surface temperature from pulse to pulse is presented in Fig. 2, calculated for 100 pulses and different repetition rates as follows

$$T_{surf} = T_0 + \frac{Q_{rem}}{\rho \cdot c}\sum_{n=1}^{n_P}\frac{1}{V_n} = T_0 + \frac{Q_{rem}}{\rho \cdot c}\left(\frac{1}{V_1}+\frac{1}{V_2}+\frac{1}{V_3}+\ldots+\frac{1}{V_{n_P}}\right) \quad (1)$$

where $\mathbf{T_{surf}}$ is the surface temperature, $\mathbf{T_0}$ is the ambient temperature, Q_{rem} is the remaining thermal energy, $\mathbf{n_P}$ is the pulse number, $\mathbf{V_n}$ is the heat affected volume of each individual pulse (determined by the time interval between the pulses), $\boldsymbol{\rho}$ is the density, and $\mathbf{c}$ is the heat capacity. The given temperature values represent the surface temperature at the end of a cooling cycle when the next laser pulse irradiates. In this calculation, enhanced energy coupling was assumed to estimate the amount of remaining energy that will be deposited within the near-surface area by every irradiated laser pulse. This assumption is based on results achieved in direct observation of temperature fields during multiple femtosecond laser ablations. For steel it was reported that a significant high fraction of incident laser power up to 70% will be deposited into the solid as thermal energy [12]. According to this, a thermal energy input of 3.5 µJ per irradiated laser pulse was taken into calculation. This is 70% of the irradiated laser pulse energy of 5 µJ.

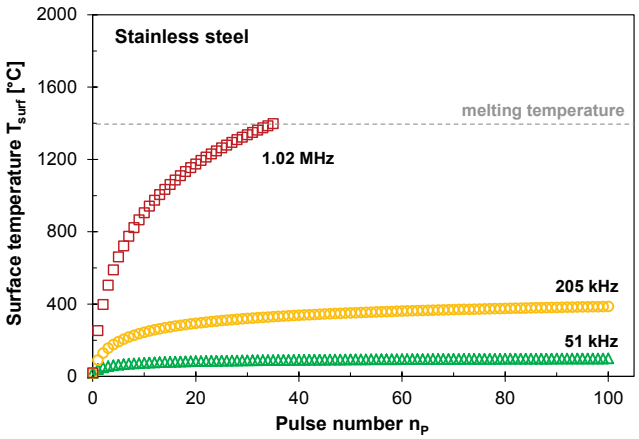

Fig. 2: Surface temperature on stainless steel calculated at the end of a cooling cycle when the next laser pulse irradiates, 100 pulses with thermal energy input of 3.5 µJ per pulse were taken into the calculation, the repetition rate was varied between 51 kHz, 205 kHz and 1.02 MHz.

In case of the lowest investigated repetition rate of 51 kHz, the surface temperature increased slightly from pulse to pulse. The maximum surface temperature obtained after 100 pulses was about 100°C. For the higher repetition rate of 205 kHz, a temperature rise up to 390°C was calculated that is considerably lower than the melting temperature of stainless steel (1,400°C). For the highest investigated repetition rate of 1.02 MHz, by contrast, Fig. 2 shows that the melting temperature of stainless steel can be reached with 35 pulses. It is assumed that this high temperature increase is mainly due to the thermal energy deposition in small near-surface areas as a result of both low heat conductivity and short time intervals between pulses of high repetition rates. Moreover, this strong temperature increase will potentially enhance laser beam absorption and lower the ablation thresholds, causing more efficient material removal. On the other hand, this study demonstrates that even ultrashort pulse laser ablation at high repetition rates is a thermal process and material melting can occur.

Particle shielding has been identified as another significant material removal influencing effect in high-PRF laser processing. Drill-through experiments revealed that the removal rate decreased for pulses with repetition rates above several hundred kilohertz [1]. This is due to the insufficient time for the ablation products to clear between the high-PRF laser pulses. As a result, the following laser pulses interact with ablated particles and droplets. Supporting this, ablation plumes induced by femtosecond laser

irradiations of stainless steel are presented in Fig. 3. A time range of 1 µs is recorded with an ultra highspeed intensified camera system (hsfc pro, PCO), correlating to the time interval of laser pulses at 1 MHz repetition rate.

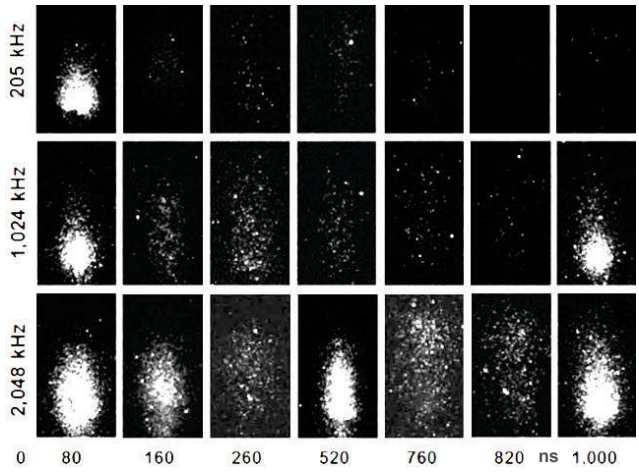

Fig. 3: Ablation plumes arising on stainless steel following femtosecond laser irradiation, pulse energy was 6 µJ; recording times after the onset of the laser pulse are given in nanoseconds.

The photographs give evidence that the ablation particle plume is still existent at the time interval one microsecond after pulse irradiation. From this, it can be concluded that high-PRF laser pulses in the range of 1 MHz or higher will be scattered, reflected and/or absorbed by the remaining ablation products, causing partially shielding of the work piece. In addition, particle shielding also affects laser beam focusing by distortion of the focused spot shape. Furthermore it can be seen in Fig. 3 that the ablation plume enlarged at the higher repetition rates as well as size and composition of the plume depend on the fluence. This is similar to results presented in an earlier work [7]. Therein it was reported that particle shielding losses have been overbalanced by heat accumulation, enhancing the material removal process.

3. Experimental

3.1 Laser systems

In this study two different high-PRF femtosecond laser systems were used. The *IMPULSE*^{TM} laser (Clark-MXR, Inc.) supplied a maximum laser power of 13.2 W at the work piece surface, whilst the maximum laser power of the *sci-series* laser (Active Fiber Systems GmbH) was 31.7 W.

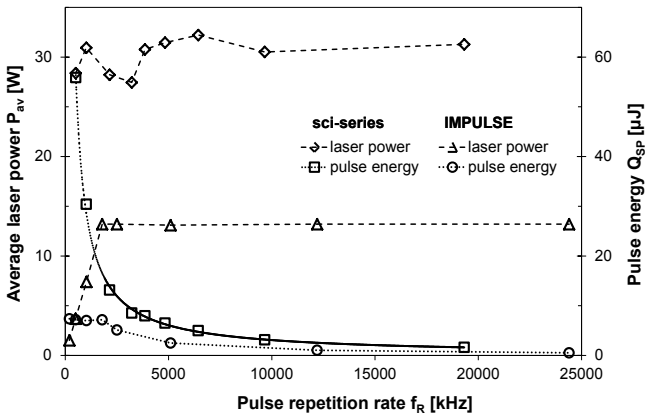

Fig. 4: Average laser power and pulse energy versus repetition rate for both the *sci-series* and the *IMPULSE* ^{TM} laser.

The maximum pulse repetition rate of both systems was in the range of 20 MHz. With increasing repetition rate, the maximum available single pulse energy decreased due to the fixed supplied maximum laser power. The proportional relation between laser power and repetition rate can be seen in Fig. 4. The most important parameters of the investigated laser systems are summarized in Table 1.

Table 1: Laser parameters; *) work piece surface.

Parameter	*IMPULSE*^{TM} (Clark-MXR)	sci-series (Active Fiber Systems)
central wave length λ	1030 nm	1030 nm
repetition rate f_R	0.2 … 24.4 MHz	0.05 … 19.3 MHz
max. laser power*) P_{av}	13.2 W	31.7 W
max. pulse energy*) Q_P	7.2 µJ	55.9 µJ
min. pulse duration τ_H	180 fs (sech^2)	350 fs (sech²)
beam propagation factor M^2	< 1.3	< 1.5

3.2 Scan systems

Two galvanometer scanner systems were utilized to deflect the laser beam across the sample surface. Compared to the *intelliSCAN 14* system, the *intelliSCANde 30* scanner provided both a considerably higher maximum scan speed and a larger scan field due to the longer focal length of the focusing objective. This is highly beneficial for prospective industrial applications of the technology providing increased processing speed, throughput, and working range. Further, strong focusing of the laser beam by the use of the *intelliSCANde 30* system produced a small focus diameter of 22µm. This was smaller than the focus diameter of 30.1 µm, achieved with the *intelliScan 14* system. Galvanometer scanner parameters are presented in Table 2.

Table 2: Galvanometer scanner parameters.

Parameter	*intelliSCAN 14* (Scanlab AG)	*intelliSCANde 30* (Scanlab AG)
focal length f	56 mm	163 mm
focus diameter $d_{0,86}$	30.1 µm	22.0 µm
max. scan speed v_S	4.5 m/s	17.1 m/s
max. scan field (width x length)	25 x 25 mm²	80 x 80 mm²
max. peak fluence on sample H_0	2.0 J/cm²	29.5 J/cm²

3.3 Materials and methodology

Two different materials have been investigated in this study, the black zirconium oxide ZrO_2, 94.5 %, partly Y_2O_3-stabilized (TZ-Black, Tosoh Corp.) and stainless steel X 5 CrNi 18-10 (1.4301, AISI 304). In these materials, standardized cavities have been produced by laser ablation using femtosecond laser pulses of various pulse repetition rate and energy. Cavity dimensions were 2 x 1 mm² in length l_X and width l_Y. The cavity depths l_Z obtained varied depending on the processing parameters.

By raster scanning, the focused laser beam was deflected across the sample surface “line-by-line” as schematical-

ly shown in Fig. 5. In scan direction, the lateral spacing $\mathbf{d_X}$ between the overlapping laser pulses was determined by the scan speed $\mathbf{v_S}$ and the repetition rate $\mathbf{f_R}$ due to the relation $\mathbf{v_S} = \mathbf{d_X} \cdot \mathbf{f_R}$. A little dither between the starting points of individual line-scans occurred (smaller than 4 µm), caused by synchronization of the laser and the galvanometer scanner. The lateral distance between the laser processed lines was given by the hatch distance $\mathbf{d_Y}$. To increase the cavity depth, multiple numbers of scan passes $\mathbf{n_S}$ were irradiated. With each investigated parameter set three distinct cavities were produced and analyzed.

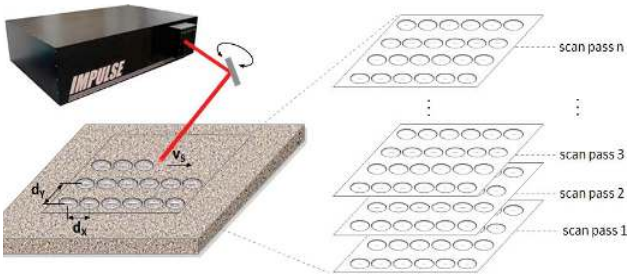

Fig. 5: Schematic of the applied scan regime, where d_X is the pulse spacing, d_Y is the hatch distance, v_S is the scan speed, and n_S is the number of scan passes.

The cavity depths were measured utilizing a measurement arrangement consisting of the *Confocam C101* (confovis) and the *LV100D–U* microscope (Nikon). The measurement data were analyzed with the Mountains Map® software. The depth of each cavity was determined by eight individual depth measurements across the cavity edge, indicated in Fig. 6 by the dotted line. A typical depth profile is shown in the lower part of Fig. 6.

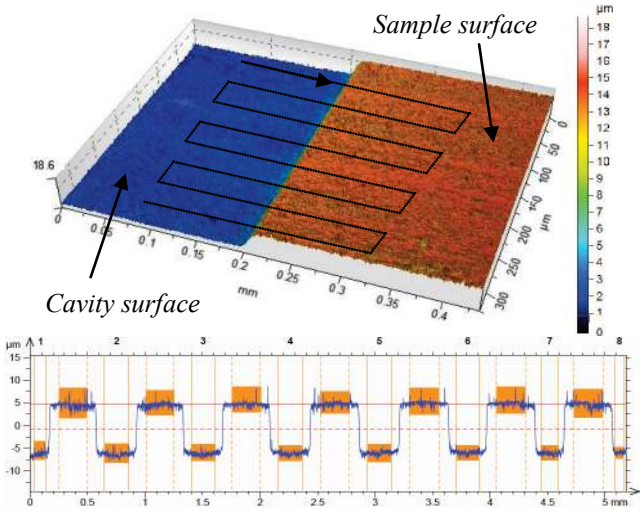

Fig. 6: Laser processed cavity and depth profile.

The mean cavity depths, averaged over three cavities fabricated with constant processing parameters were used to evaluate the impact of the processing parameter on material removal. In (2), the cavity depth $\mathbf{l_Z}$ is used to determine the ablation rate $\mathbf{d_P}$. The ablation rate denotes the mean ablation depth per incident laser pulse. In this calculation, the average number of incident laser pulses per area was considered by taking into account the focus radius $\mathbf{w_0}$.

$$d_P = \frac{l_Z \cdot d_X \cdot d_Y}{n_S \cdot \pi \cdot w_0^2} \qquad (2)$$

In addition, (3) gives the volume ablation rates $\mathbf{V_P}$ as the removed material volume per irradiated laser pulse. In this calculation, the laser ablated cavity volume is related to the total number of irradiated laser pulses $\mathbf{n_t}$ by taking into calculation the cavity depth $\mathbf{l_Z}$.

$$V_P = \frac{V_{tot}}{n_t} = \frac{l_X \cdot l_Y \cdot l_Z}{n_t} = \frac{d_X \cdot d_Y \cdot l_Z}{n_S} \qquad (3)$$

Finally, scaling of the volume ablation rate with the repetition rate yields the material removal rate **MRR** as the removable material volume per time.

$$\mathrm{MRR} = V_P \cdot f_R \qquad (4)$$

4. Results and discussion

4.1 Zirconium oxide TZ-Black

Laser ablation of zirconium oxide TZ-Black was studied utilizing the *IMPULSE™* laser in combination with the *intelliSCAN 14* scan system. By using this setup, the maximum pulse energy supplied to the sample was 7.2 µJ, correlating to the peak fluence of 2.0 J/cm². The pulse repetition rate and the pulse spacing were varied in the range between 20 kHz and 1.02 MHz, and 2 µm and 6 µm, respectively. The hatch distance was kept constant of 4 µm during the experiments; the number of scan passes was 25.

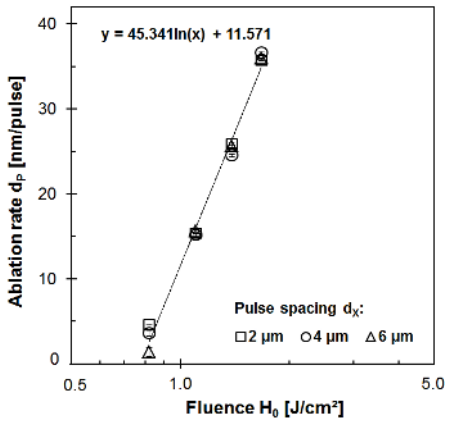

Fig. 7: Ablation rate versus fluence obtained on zirconium oxide TZ-Black, the pulse spacing was varied in the range between 2.0 and 6.0 µm, the repetition rate was 20 kHz.

Fig. 7 presents the semi logarithmic plot of the ablation rate as a function of the fluence. The repetition rate was 20 kHz and the pulse spacing was varied between 2 µm and 6 µm. The ablation rate increased logarithmically with higher laser fluence and was almost unaffected by the pulse spacing. Thus, the results achieved in this processing parameter range indicate no significant impact of heat accumulation and/or particle shielding on material ablation. Further, from the regression line given in the plot, a laser energy penetration depth of 45 nm can be derived.

In addition, the volume ablation rates have been determined from the cavity depths by using (3). The pulse spacing was kept constant of 4 µm. The results obtained for 20 kHz correlate closely to theoretically achieved volume ablation rates, calculated by using a method introduced in [13]. The effective penetration depth of 45 nm, as derived from Fig. 7, and the ablation threshold of 0.48 J/cm² were used in this calculation.

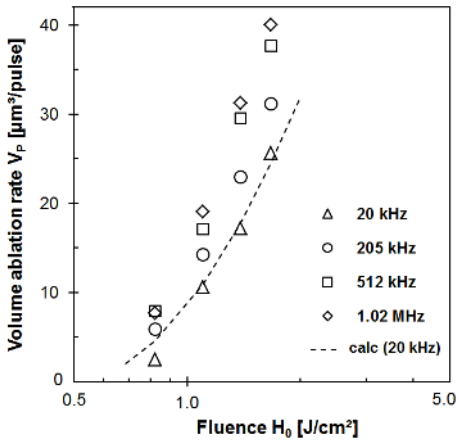

Fig. 8: Volume ablation rate versus fluence obtained on zirconium oxide TZ-Black, the repetition rate was varied in the range between 20 kHz and 1.02 MHz, the pulse spacing was 4.0 µm.

In Fig. 8 it can be seen that the ablation volume rate increases with the higher pulse repetition rate. For this, heat accumulation can be supposed as mainly influencing effect, causing enhanced interaction of the ceramic with the laser beam. In addition, the surface temperature might come into play because of the dependence of both absorptivity and heat conduction on the temperature has been reported for different ceramics [14]. However, thermal impact on both thermo-physical and optical material properties of zirconium oxide has not been fully clarified in this study, and further work is needed here.

Fig. 9 emphasizes the assumption that heat accumulation will enhance material removal on zirconium oxide. Volume ablation rates are given versus pulse spacing; the pulse repetition rate and pulse energy were varied. As already mentioned, material processing using laser pulses at low repetition rates is almost unaffected by heat accumulation. As a first indication for this, almost constant volume ablation rates can be recognized in Fig. 9 for pulses at 20 kHz and varying pulse spacing.

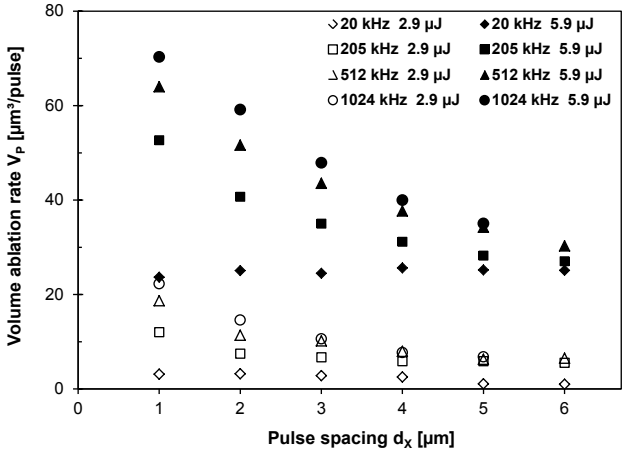

Fig. 9: Volume ablation rate versus fluence obtained on zirconium oxide TZ-Black; both the pulse spacing and the repetition rate were varied.

By contrast, the ablation volume increased considerably with higher repetition rates and smaller pulse spacing. In addition, the volume ablation rates strongly enlarged with the higher pulse energy of 5.0 µJ, compared to 2.9 µJ.

The maximum achieved volume ablation rate was 70.3 µm³ per pulse, obtained with 5.9 µJ at 1.02 MHz and 1 µm pulse spacing. Scaling of this value with the repetition rate of 1.02 MHz yields the maximum possible material removal rate of 4.3 mm³ per minute. However, a high thermal load of the work piece occurred with this parameter set causing thermal stresses. As a result, micro crack formation appeared at the bottom of the laser processed area, shown in Fig. 10 (top left). The mere enlargement of the pulse spacing to 2 µm reduced the crack formation considerably, observable in Fig. 10 (top right). Along with this, the maximum achievable material removal rate decreased to 3.6 mm³ per minute due to the lower thermal load.

The SEM photograph of a machining sample made in zirconium oxide TZ-Black is presented in the lower part of Fig. 10. The processing parameters were as follows: 5.0 µJ pulse energy, 2 µm pulse spacing, 4 µm hatch distance, and 1.02 MHz repetition rate. Structure dimension were 1 x 1 mm² in width and length. The width of the inner cross walls was 60 µm on the sample surface, and enlarged with increasing structure depth. A maximum depth of 167 µm was achieved with 25 scan passes. The processing time to fabricate this demonstrator by using bidirectional scanning of the laser beam was 19.7 seconds.

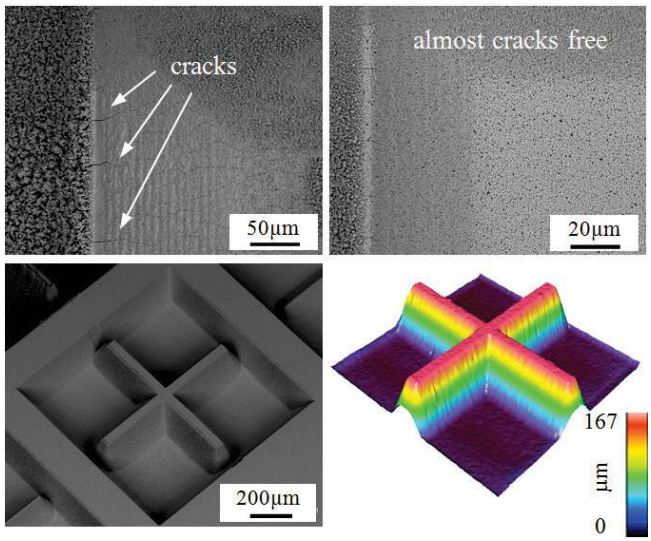

Fig. 10 top: SEM images of wall edges obtained on zirconium oxide TZ-black with 5.9 µJ at 1.02 MHz and either 1 µm (left) or 2 µm (right) pulse spacing, micro cracks can be seen in the left picture; **bottom:** demonstrator structure in zirconium oxide TZ-Black presented as SEM micrograph (left) and 3D measurement (right).

For comparison, this demonstrator structure was processed with lowered repetition rates and, in turn, lowered scan speeds (to provide similar pulse spacing of 2 µm); all other processing parameters were kept constant. By using the lower repetition rate of 205 kHz, the processing time increased to 30.5 seconds, and 160 seconds were needed with the lowest investigated repetition rate of 20 kHz. It is obvious that the processing time scales non-linearly with the scan speed. This is due to extra times that will be in raster scan processing to move the laser beam from the end point of the laser processed line to the start point of the new scan line to be processed. Moreover, by using a process regime introduced in [15], acceleration and deceleration sections were added to the processing path. This is to

avoid pulse accumulation at the edges of the structure. The lengths of these sections strongly depend on the scan speed.

However, for the low repetition rates it was mentioned already that material removal benefits less or not at all from heat accumulation. Thus, significantly lower depths of the demonstrator were obtained with the lower repetition rates, such as 125 µm at 205 kHz, and 110 µm at 20 kHz, respectively.

4.2 Stainless steel X5CrNi 18-10 (1.4301, AISI 304)

High-PRF laser processing of stainless steel was intensively studied in our previous works within the parameter range up to 7.2 µJ pulse energy, or rather 2.0 J/cm² fluence, and 1.02 MHz pulse repetition rate by using the *IMPULSE™* laser [5-7, 9, 15]. In these studies the increase of the ablation rate due to enhanced laser beam absorption and lowered ablation threshold initiated by heat accumulation has been demonstrated.

In this work, high-PRF laser processing of stainless steel was studied using a high laser power of 31.7 W, supplied by the *sci-series* laser. With this laser power, the ablation threshold can be exceeded even by irradiating ultrashort pulses at high repetition rates in the range up to 20 MHz. The laser system was used in combination with the *intelliSCANde 30*, providing much faster scan speeds than the scan system used in previous experiments. The study aimed to investigate the impact of the higher laser power on both material ablation and processing speed. Another goal was the enlargement of the processing area by using a longer focus distance objective.

The maximum available laser power of 31.7 W was irradiated on the work piece surface to fabricate standardized cavities as mentioned above. The repetition rate was varied and, as a result, laser pulses at lower fluence irradiated at the higher repetition rates. The maximum available laser power varied slightly with the repetition rates, as shown in Fig. 4.

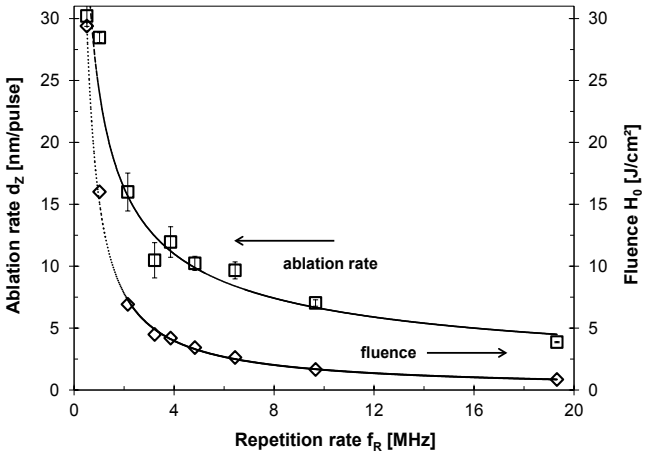

Fig. 11: Ablation rate and fluence versus repetition rate obtained on stainless steel.

Fig. 11 plots the ablation rate versus the repetition rate. Furthermore, the functional dependence of the fluence on the repetition rate is presented. The ablation rate was calculated by using (2) and taking into account the cavity depths obtained. The maximum ablation rate of 30.2 nm / pulse was achieved with pulses of 29.4 J/cm². This was the highest investigated fluence, available at 508 kHz repetition rate. The ablation rate decreased with higher repetition rates, potentially affected by the lower fluence.

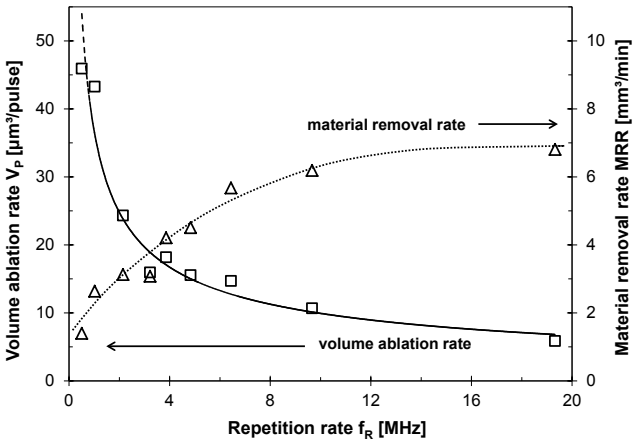

Fig. 12: Volume ablation rate and material removal rate versus repetition rate obtained on stainless steel.

The functional correlation between the volume ablation rate versus the repetition rate is presented in Fig. 12. The plot indicates the decrease of the volume ablation rate with higher repetition rate that is in accordance with Fig. 11. Further, the material removal rate is given, calculated by scaling of the volume ablation rate with the repetition rate accordingly (4). It can be seen that the material removal rate increased with the higher repetition rate, in spite of the decreasing amount of material that was removed per laser pulse. The maximum material removal rate was found to be 6.8 mm³ / min, achieved with laser pulses of 0.85 J/cm² and 19.3 MHz. This fluence of 0.85 J/cm² is almost eight times above the ablation threshold of stainless steel, which has been determined previously of $H_{th} = 0.1$ J/cm². According to this, it is noteworthy that the highest ablation efficiency was reported for laser pulses with fluence of about 7.4 times above the ablation threshold [16].

SEM micrographs of laser processed cavity surfaces obtained with different fluence are summarized in Fig. 13. In all cases, almost the same laser power was irradiated. The fluence decreased depending on the increase of the pulse repetition rate. It can be seen that the surface quality was strongly influenced by the processing parameters.

The best machining quality was reached with the lowest investigated fluence of 0.85 J/cm² and the highest repetition rate of 19.3 MHz. The laser processed surface appeared smooth without any micro craters, and neither redeposited ablation products (debris) nor molten bulges can be seen. A minor heat load of the work piece can be suggested in spite of the high irradiated laser power. This might be due the low fluence of the irradiated laser pulses and the high processing speed.

Furthermore, it can be seen in Fig. 13 that laser processing with laser pulses of higher fluence and lower repetition rates will potentially cause rough surfaces. The cavity bottoms were littered with micro craters, re-deposited ablation products, as well as molten and re-solidified fragments. By contrast, highly regular and smooth cavity surfaces have been achieved with the highest irradiated fluence of 29.4 J/cm² and the lowest repetition rate of 508 kHz. However, a number of deep micro craters appeared randomly at the laser processed surface.

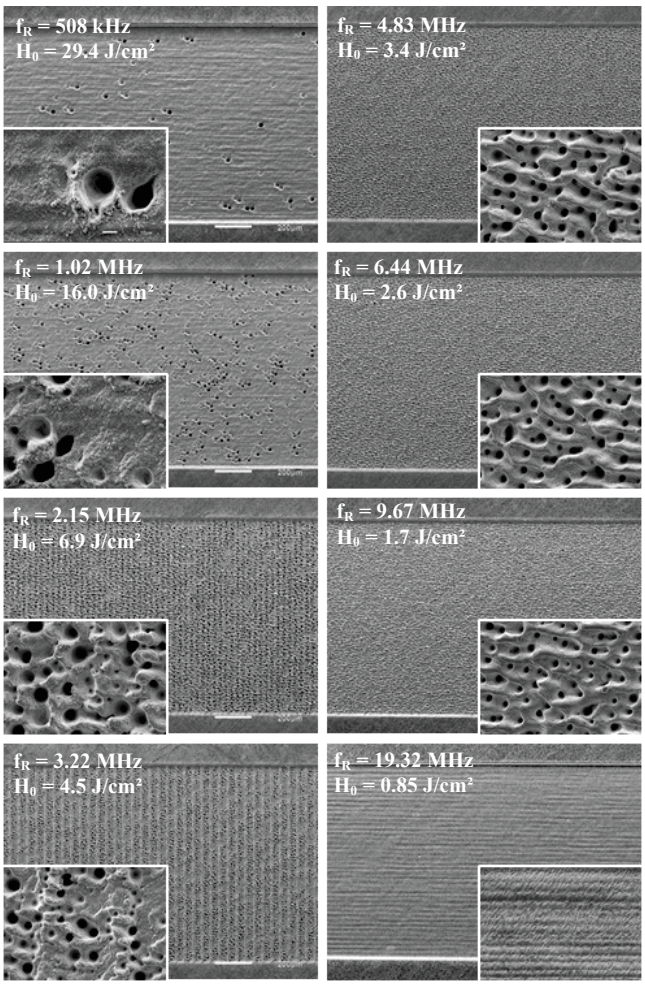

Fig. 13: SEM micrographs of laser processed cavity surfaces obtained with increasing repetition rates and decreasing fluence, the cavity width was 1 mm.

Fig. 14 presents white light illumination of a rectangular diffraction pattern, laser processed on stainless steel with the dimension of 80 x 80 mm² in width and length. Ripple formation can be observed in the small picture.

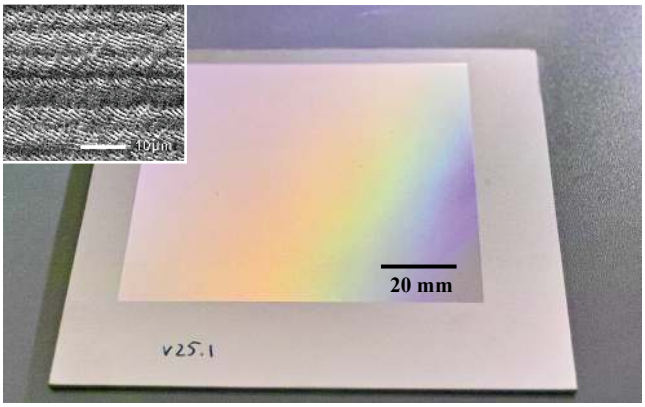

Fig. 14: Rectangular diffraction pattern of 80 x 80 mm² (width x length) achieved on stainless steel, processing parameters were: 1.0 J/cm² fluence, 3.2 MHz repetition rate, 11.3 m/s scan speed, 5 µm hatch distance and 1 scan pass.

This sample was fabricated with laser pulses of 1.0 J/cm² and 3.2 MHz repetition rate. The pulse spacing was 3.5 µm and the scan speed 11.3 m/s, respectively. The hatch distance was 5 µm and acceleration / deceleration sections were applied. The processing time for one laser pass in total was 157 seconds. As a result, a processing rate of 25 cm²/min was achieved. This is about three times faster than processing rates demonstrated before by utilizing the *intelliSCAN 14* system. The processing area of the latter scanner configuration was smaller than 25 x 25 mm² with a maximum processing rate of about 8 cm²/min.

Summary

Highspeed laser processing of zirconium oxide TZ-Black and stainless steel was studied. Two different high-PRF femtosecond laser systems were utilized in combination with fast galvanometer scanner systems.

Zirconium oxide TZ-Black was irradiated with a maximum laser power of 7.2 W. The pulse energy, the repetition rate and the pulse spacing were varied. A significant impact of heat on material removal was identified. The maximum achieved volume ablation rate was 70.3 µm³ per pulse, obtained with 5.9 µJ at 1.02 MHz and 1 µm pulse spacing. Scaling of this value with the repetition rate of 1.02 MHz yields the maximum material removal rate of 4.3 mm³ per minute. By irradiating laser pulses with this small spacing of 1 µm, crack formation was observed on the walls of a micro-featured demonstrator. This might be caused by thermal stresses.

The maximum available average laser power of 31.7 W was irradiated on stainless steel. The repetition rate was varied, inducing the decrease of the applied fluence. The maximum ablation rate of 30.2 nm/pulse was achieved with pulses of 29.4 J/cm² at 508 kHz. The maximum material removal rate of 6.8 mm³/min, by contrast, was achieved with laser pulses of 0.85 J/cm² and 19.3 MHz. The high processing speed was demonstrated by means of a diffraction pattern. This rectangular demonstrator of 80 x 80 mm² was processed with a processing rate of 25 cm²/min.

Acknowledgments

The presented results have been conducted in the course of the projects ”Innoprofile Transfer – Rapid Micro/Hochrate-Laserbearbeitung” (03IPT506X), funded by the Federal Ministry of Education and Research, “Fabrication and investigations of spintronic layer systems – Spintronic”(60714/226), funded by the European Union (European Regional Development Fund – EFRE) and the Free State of Saxony, Germany, and the CLUSTER project “Gecko TP-V Reibwerterhöhende Laserstrukturierung" (AiF 17228 BR/1), funded by the Federal Ministry of Economics and Technology. Further the authors gratefully acknowledge Felix Dreisow for his assistance in using the *sci-series* laser.

References

[1] A. Ancona, F. Roeser, K. Rademaker, J. Limpert, S. Nolte and A. Tuennermann: Optics Express, 16 (12), (2008) 8958.

[2] S. Doering, A. Ancona, S. Haedrich, J. Limpert, S. Nolte and A. Tuennermann: Applied Physics A, 100 (1), (2010) 53.

[3] S. Nolte, S. Doering, A. Ancona, J. Limpert and Andreas Tuennermann: Advances in Optical Materials, OSA Technical Digest (CD) (Optical Society of America, (2011) FThC1.

[4] B. Tan, S. Panchatsharam and K. Venkatakrishnan: Journal of Physics D: Applied Physics, 42 (6), (2009) 065102.
[5] J. Schille, R. Ebert, U. Loeschner, P. Regenfuss, T. Suess and H. Exner: Proc. 9th Int. Symp. on Laser Precision Microfabrication, Quebec (Canada), (2008) Paper 08_027.
[6] J. Schille, L. Schneider, U. Loeschner, R. Ebert, P. Scully, N. Goddard, B. Steiger and H. Exner: Proc. of 30th Int. Congress on Appl. of Lasers and Electro-Optics, Orlando (USA), (2011) #M102.
[7] J. Schille, L. Schneider, L. Hartwig, U. Loeschner, R. Ebert, P. Scully, N. Goddard, H. Exner: Proc. of 31th Int. Congress on Appl. of Lasers and Electro-Optics, Anaheim (USA), (2012) 949.
[8] P.W. Chan, Y.W. Chan and H.S. Ng: Physics Letters A, 61 (3), (1977) 151.
[9] J. Schille: "Investigation of micromachining using a high repetition rate femtosecond fibre laser", Thesis, Manchester, UK: The University of Manchester, (2013).
[10] S. Panchatsharam, B. Tan and K. Venkatakrishnan: Journal of Applied Physics, 105, (2009) 093103.
[11] R. Le Harzic, F. Stracke and H. Zimmermann: Journal of Applied Physics, 113, (2013) 183503.
[12] D.V. Tran, Y.C. Lam, H.Y. Zheng, B.S. Wong and D.E. Hardt: Applied Surface Science, 253 (17), (2007) 7290.
[13] B. Neuenschwander, G.F. Bucher, C. Nussbaum, B. Joss, M. Muralt, U.W. Hunziker and P. Schuetz: LAMOM Photonics West, (2010) 7584-26.
[14] A.N. Samant and N.B. Dahotre: Int. Journal of Applied Ceramic Technology, 8 (1), (2011) 127.
[15] J. Schille, R. Ebert, U. Loeschner, L. Schneider, N. Walther, P. Regenfuss, P. Scully, N. Goddard and H. Exner: Proc. 5th Int. Congress on Laser Advanced Materials Processing, Kobe (Japan), (2009) #151.
[16] G. Raciukaitis, M. Brikas, P. Gecys, B. Voisiat and M. Gedvilas: JLMN Journal of Laser Micro/Nanoengineering, Vol. 4 (3), (2009) 186.

(Received: August 27, 2013, Accepted: May 13, 2014)